Journal of Power Sources 249 (2014) 446–456

Contents lists available at ScienceDirect

Journal of Power Sources

journal homepage: www.elsevier.com/locate/jpowsour

Modelling of the vapour–liquid equilibrium of water and the in situ concentration of H_3PO_4 in a high temperature proton exchange membrane fuel cell

Timur J. Kazdal*, Sebastian Lang, Frank Kühl, Manfred J. Hampe

Technische Universität Darmstadt, Thermische Verfahrenstechnik, Darmstadt, Germany

HIGHLIGHTS

- Implementation of the vapour liquid equilibrium of water/phosphoric acid.
- Implementation of evaporation kinetics for water.
- Calculation of the in situ concentration of phosphoric acid.
- Concentration dependent ionic conductivity, diffusivity and vapour pressure.
- Implementation of acid volume change affecting the porosity in the catalytic layers.

ARTICLE INFO

Article history:
Received 29 April 2013
Received in revised form
10 October 2013
Accepted 15 October 2013
Available online 5 November 2013

Keywords:
HT PEM
Water cross-over
Fuel cell modelling
PBI
Phosphoric acid thinning

ABSTRACT

The fuel cell technology is a key element for the hydrogen energy economy and therefore crucial for sustainable development. High temperature proton exchange membrane (HT-PEM) fuel cells (FC) can be operated with reformate gas and thus represent an important bridging technology for the energy transition to a renewable energy based system. HT-PEM FCs based on phosphoric acid (PA) are still subject to intense research, investigating the electrolyte behaviour. By enhancing state of the art 2D FEM simulations of FCs with the vapour liquid equilibrium of water–phosphoric acid and evaporation kinetics, a model was created in which the local concentration of PA can be calculated. Knowledge of the concentration field yields the basis for calculating the locally varying ionic conductivity and other physical properties. By describing the volume expansion behaviour of PA it was possible to predict the catalyst particle deactivation due to the swelling of PA. The in situ concentration predicted by the simulation ranges from 96 to 111 wt%. The model was validated using measured data of a single cell design for different temperatures and pressures. By varying the PA content flooding of the simulated fuel cell could be observed and was linked to humidification effects.

1. Introduction

Fuel cells are efficient energy converters that convert the chemical energy of a fuel into electrical energy. In addition to high conversion efficiency compared to conventional technology the key advantage of fuel cells is the possibility of a renewable fuel. The usage of hydrogen from renewable sources yields zero emissions, local as well as global.

The market shows rapidly growing interest in the transport sector. For stationary applications the first product lines are already available: Fuel cells equipped with internal gas reformers generating both power and heat. The mentioned application as a micro combined heat and power system is of great importance for Germany [1]. The operation of the micro-CHP with substitute natural gas from renewable sources is one of the first major milestones in the energy transition. The usage of renewable synthetic gas requires gas-to-power technologies and places high demands on the flexibility of the power converter, especially with respect to the fuel. HT PEM FCs are, because of their high CO tolerance [2], suitable for use with H_2-rich synthetic natural gas. Furthermore, they also achieve excellent efficiency.

The critical component of a FC is the membrane electrode assembly. Recent research focuses on phosphoric acid doped polybenzimidazole (PBI) membranes for HT PEM FC applications [3,4]. These have the advantage of being ionically conductive at low relative humidity and therefore auxiliary equipment regarding

* Corresponding author.
E-mail address: kazdal@tvt.tu-darmstadt.de (T.J. Kazdal).
URL: http://www.tvt.tu-darmstadt.de/

0378-7753/$ – see front matter © 2013 Elsevier B.V. All rights reserved.
http://dx.doi.org/10.1016/j.jpowsour.2013.10.098

Nomenclature

k_B	Boltzmann constant
α	transfer coefficient
ΔH_r°	standard reaction enthalpy
δ	diffusion length
η_{act}	activation polarization
γ	pressure coefficient
κ_{br}	permeability
λ_i	stoichiometric coefficient
$\mathfrak{D}_{ik}$	binary diffusion coefficient
μ	dynamic viscosity
ω	mass fraction
ϕ	volume fraction
ρ	density
σ	conductivity
τ	tortuosity
Θ_{active}	ECSA per volume catalyst
Θ_{incorp}	incorporated platinum area
ε	porosity
$B_{electrode}$	electrode thickness
C_i	concentration
c_p	heat capacity
D_{ik}	diffusion coefficient
d_{pt}	diameter platinum particle
E	electrode potential
E_A	activation energy
F	Faraday constant
H_i	Henry coefficient
i_0	exchange current density
k	thermal conductivity
L_{cat}	catalyst loading
M_i	molar mass
N_A	Avogadro's number
p	pressure
p_{vp}	vapour pressure
Q	heat source/sink
R	gas constant
R_i	species source/sink
R_{cat}	electrode roughness
ref	reference
T	temperature
u	velocity
V_m	molar volume
X	doping level
x_i	mole fraction
A	area
carb	carbon black
CL	catalytic layer
ECSA	electrochemical active surface area
GDL	gas diffusion layer
HOR	hydrogen oxidation reaction
j	current density
m	mass
MEA	membrane electrode assembly
No.	number of
ORR	oxygen reduction reaction
PA	phosphoric acid
PAM	phosphoric acid mixture
PBI	polybenzimidazole
PC	phase change
STP	standard conditions for temperature and pressure
TGA	thermogravimetric analysis

humidification is assumed to be omittable [5]. However, many physical properties of phosphoric acid, as well as the ionic conductivity, are a function of the water content in the acid [6–8]. Unlike for low temperature (LT) PEM FCs, for the high temperature (HT) PEM FCs only very few studies on the water balance were performed.

In the literature, many approaches to model HT [9,10] PEM FCs [11,12] can be found. Until now, the distribution of phosphoric acid was not subject to the investigations. Within this paper the 2D model of a HT PEM FC with a PBI membrane electrode assembly (MEA) is presented. Special emphasis lies on the water balance in the membrane. Understanding the balance is crucial for the proper simulation of HT PEM FCs because the assumption of constant, water independent physical properties is not necessarily valid. With a model for the vapour liquid equilibrium the water household of the FC was calculated. On the basis of the obtained distribution of water, the physical parameters of the electrolyte were determined. Moreover, the sorption behaviour of PA was investigated and its volume expansion and thus the pore filling degree was implemented into the model. Since a flooded pore is assumed to be electrochemically deactivated, the reaction kinetics were, in consequence, coupled with the local concentration of water.

2. Model

2.1. Model description and assumptions

In this work a 2D model of a high temperature PEM fuel cell is presented. The calculation domain consists of gas channels, gas diffusion layers, catalytic layers and a membrane, as seen in Fig. 1. The dimensions are summarized in Table 1. The following assumptions were made:

2.1.1. General

- Anisothermal
- Steady state
- ORR dominates activation overpotentials
- No gas permeation through the membrane → no mixed potential
- Operation on hydrogen and air
- Ideal gas mixtures in gas phase

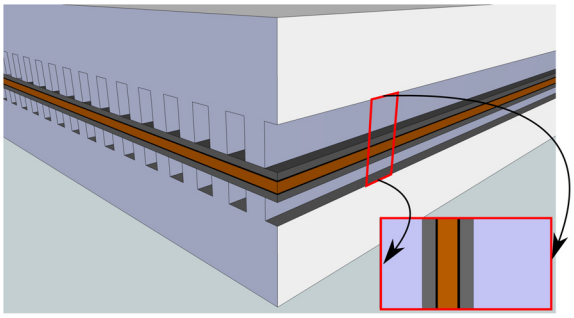

Fig. 1. Sketch of two sectional planes through the single cell with highlighted calculation domains.

Table 1
Model dimensions.

Thickness	
H_2 channel	1.07 [mm]
Anode GDL	0.34 [mm]
Anode	0.05 [mm]
Membrane	0.11 [mm]
Cathode	0.06 [mm]
Cathode GDL	0.34 [mm]
Air channel	1.96 [mm]
Channel depth	1.19 [mm]
Channel length	1050 [mm]

2.1.2. Materials

- Macro homogeneous and isotropic
- Pore size distribution in the catalytic layer has two maxima
- Effect of porosity on transport parameters is described by the Bruggemann correlation

2.1.3. Phosphoric acid

It is assumed that phosphoric acid polymerises as described by R.F. Jameson [13]. In his work he presents the equilibrium concentrations of the polyphosphoric acids at 15 °C. To account for the temperature dependence of the reaction equilibrium we used data from R.A. Munsen [14,15]. He studied the kinetics of the ortho-pyro interconversion and found the equilibrium constant to be of the magnitude of E-03 in the range of 40–100 °C. Therefore it is reasonable to neglect the temperature dependence and to use Jameson's data for the estimation of the composition distribution while discussing the concentration of PA.

Furthermore for the physical properties of phosphoric acid the effects of this polymerization are accounted for by the implementation of the concept of apparent concentrations: A mixture of 90 wt%[1] phosphoric acid heated to 200 °C in a closed system has a metrological determinable ionic conductivity. Its value is related to the temperature and the apparent concentration of 90 wt% PA, despite the fact that polycondensation might have occurred. This concept was applied to all empirically determined physical properties.

- no polycondensation thermodynamics and kinetics of phosphoric acid
  - Only one species → concept of apparent concentration
  - Physical properties (D,σ,p_{vp}) still account for polycondensation and the actual, but unknown composition
- Diffusion coefficient of PA depends on temperature and concentration
- Vapour pressure of species PA is neglected. At 221 °C E.H. Brown [16] observed a mass fraction of 0.9 wt% in the vapour phase.
- Acid expansion and contraction is completely reversible during one simulation run
- Capillarity does not affect evaporation

2.1.4. PBI-membrane

- Contains free acid and can be considered as a porous medium
- No thickness change over lifetime
- No volume swelling during a simulation run. Assuming that the amount of PA is constant during a simulation run, only water enters and leaves the membrane. R. He [17] studied the influence of the doped acid and absorbed water on the volume swelling for acid doped PBI membranes and found the effect of swelling by water to be negligible
- Ionic conductivity and diffusion coefficient depend on acid concentration, temperature and morphology (ε, τ)
- Water gradient through the membrane is of higher magnitude than along the channel

In Fig. 2 the magnified model geometry is shown and the naming convention for the domains and the boundaries is presented. The governing equations and their computational domains are summarized in Fig. 3.

2.2. Governing equations

2.2.1. Conservation of mass and momentum

The velocity field is obtained by solving the equation of continuity in combination with the Navier–Stokes and the Brinkman equations for flow in porous media. It is important, to mention the porosity dependence of Brinkman's equation, as seen in EQ:1, because Chapter 2.3 will introduce the porosity in the catalytic layer as a dependent variable.

$$\frac{\rho}{\varepsilon}\left(u\cdot\nabla\left(\frac{u}{\varepsilon}\right)\right)=\nabla\left[-pE+\frac{\mu}{\varepsilon}\left(\nabla u+(\nabla u)^T\right)-\frac{2\mu}{3\varepsilon}(\nabla u)E\right]-\left(\frac{\mu}{\kappa_{br}}+\dot{m}\right)u \tag{1}$$

There are two convective mass flows to consider, one in each channel. The gas diffusion layers (GDL, [2] & [6]) and the catalytic layers (CL, [3] & [5]) are modelled as porous media. The energy balance and the conservation of species are coupled with the conservation of mass, to account for the change of density and temperature. Table 2 shows parameters for calculating the conservation of mass and momentum.

2.2.1.1. Boundary conditions. u_{HOR} and u_{ORR} are flow velocities. For stoichiometric operation the velocities depend on the current generated and the cell geometry according to EQ:2:

$$u_{HOR}=\frac{1}{No._{Channels}\cdot A_{Channel}}\cdot\frac{j_{HOR}\cdot A_{Cell}\cdot R\cdot T\cdot\lambda_{Ano}}{2F\cdot p_{HOR}\cdot x_{H_2}} \tag{2}$$

2.2.1.2. Source terms. At both electrodes mass is produced and consumed. The two effects considered are the reaction conversion

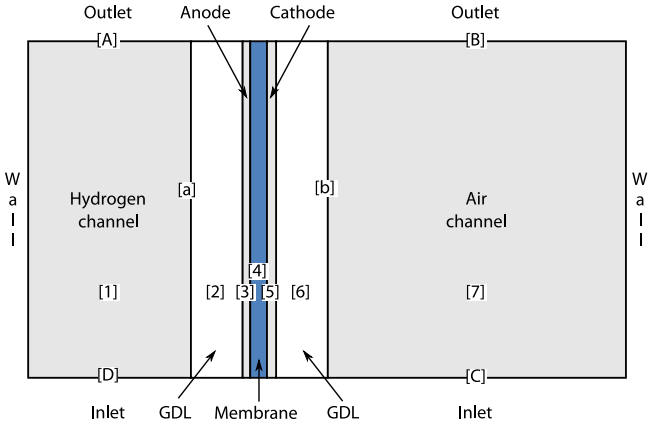

Fig. 2. Model geometry and naming convention.

[1] Consists of 100% ortho-PA @ 15 °C [13].

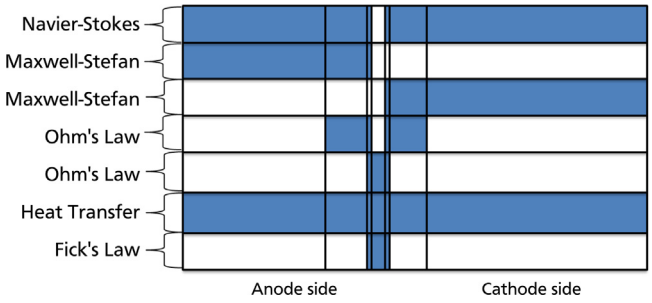

Fig. 3. Governing equations and their calculation domains.

and the phase change. Reaction conversion is directly related to the electrical flux, as seen in EQ:3 and EQ:4. The change of mass due to phase change will be introduced in Section 2.3.

$$\dot{m}_{\mathrm{HOR}} = j_{\mathrm{HOR}}\frac{M_{\mathrm{H_2}}}{2F} \tag{3}$$

$$\dot{m}_{\mathrm{ORR}} = j_{\mathrm{ORR}}\left(\frac{M_{\mathrm{H_2O}}}{2F} - \frac{M_{\mathrm{O_2}}}{4F}\right) \tag{4}$$

2.2.2. Conservation of species

The Stefan–Maxwell equation (EQ:6) is used to model the conservation of species. By solving the equations for the conservation of mass and momentum the convective velocity u is provided. The density within gaseous phases is calculated by the ideal gas law. For the calculation of the Stefan–Maxwell diffusion coefficients for a three component system EQ:7 [18] can be used. The binary diffusion coefficients are calculated by EQ:8 [18] and EQ:9 [19] respective their validity[2] and corrected by the Bruggeman equation (EQ:11) [20] regarding the porosity of the respective domain material.

$$\nabla j_i + \rho(u\nabla)\omega_i = R_i \tag{5}$$

$$j_i = -\left(\rho\omega_i \sum_{k=1} D_{ik}\nabla\omega_k\right) \tag{6}$$

$$D_{ik} = \frac{\dfrac{\omega_i(\omega_k+\omega_m)}{x_i\mathfrak{D}_{km}} + \dfrac{\omega_k(\omega_i+\omega_m)}{x_k\mathfrak{D}_{im}} - \dfrac{\omega_m^2}{x_m\mathfrak{D}_{ik}}}{\dfrac{x_i}{\mathfrak{D}_{ik}\mathfrak{D}_{im}} + \dfrac{x_k}{\mathfrak{D}_{ik}\mathfrak{D}_{km}} + \dfrac{x_m}{\mathfrak{D}_{im}\mathfrak{D}_{km}}} \tag{7}$$

$$\mathfrak{D}_{\mathrm{H_2}k} = \frac{0.00143}{\sqrt{2}p}\frac{T^{1.75}}{\left[\left(\sum v_{\mathrm{H_2}}\right)^{\frac{1}{3}} + \left(\sum v_k\right)^{\frac{1}{3}}\right]^{\frac{1}{2}}}\left(\frac{1}{M_{\mathrm{H_2}}} + \frac{1}{M_k}\right)^{\frac{1}{2}} \tag{8}$$

$$\mathfrak{D}_{ik} = \frac{a}{p}\left(p_{c,i}p_{c,k}\right)^{\frac{1}{3}}\left(T_{c,i}T_{c,k}\right)^{\frac{5}{12}}\left(\frac{1}{M_i} + \frac{1}{M_k}\right)^{\frac{1}{2}}\left(\frac{T}{\sqrt{T_{c,i}T_{c,k}}}\right)^{b} \tag{9}$$

2.2.2.1. Sources. The source terms are equal to those presented in Section 2.2.1. For the conservation of species they are mapped to the reacting species. E.g. the mass loss in the anode is a loss of the species hydrogen (Table 3).

[2] EQ:8 for binary diffusion coefficients of mixtures containing hydrogen.

Table 2
Parameter, boundary and initial values regarding the conservation of mass and momentum.

Domain	Important parameter
[2]	$\varepsilon^{[2]} = 0.4$
[3]	$\varepsilon^{[3]} = \varepsilon(T,\omega_{\mathrm{PA}})$
[5]	$\varepsilon^{[5]} = \varepsilon(T,\omega_{\mathrm{PA}})$
[6]	$\varepsilon^{[6]} = 0.4$
Domain	**Initial value**
[1]	u_{HOR}
[7]	u_{ORR}
[1],[2],[3]	p_{HOR}
[5],[6],[7]	p_{ORR}
Boundary	**Condition**
[A]	p_{HOR}
[B]	p_{ORR}
[C]	u_{ORR}, laminar inflow
[D]	u_{HOR}, laminar inflow
Source	**Term**
[3]	$\dot{m}_{\mathrm{HOR}} + \dot{m}_{\mathrm{PC}}^{[3]}$
[5]	$\dot{m}_{\mathrm{ORR}} + \dot{m}_{\mathrm{PC}}^{[5]}$

2.2.3. Conservation of charge

2.2.3.1. Electron flux. The approach for describing the electrical flux can be divided into two regions: anode and cathode. Each region has an electron source and a boundary condition where the potential is constant, creating a potential field over the domain. Combining this potential field with the electrical conductivity leads to an electron flux. As seen in Table 4 the potential field is introduced between the two interior boundaries [a] and [b]. Current sources are the two catalytic layers [3] and [5] with the hydrogen oxidation reaction as the source for electrons and ions and the oxygen reduction reaction as the sink for both species. We use the Bruggeman equation [20] to correct the electrical conductivity of the catalytic and gas diffusion layers with respect to their carbon volume fraction. Electrons are produced in the catalytic layer of the anode [3] and with the lower potential at [a] we obtain the electrical flux for the anode side. At the cathode the charge travels from the place of higher potential [b] to the sink at the catalytic layer of the cathode [5], where the reaction consumes them (Tables 5).

$$j = \sigma E + j_{\mathrm{e}} \tag{10}$$

Table 3
Parameter, boundary and initial values regarding the conservation of species.

Domain	Initial value
[1], [2], [3]	$\omega_{\mathrm{H_2}} = 1 - \omega_{\mathrm{H_2O}}$
[5], [6], [7]	$\omega_{\mathrm{O_2}} = 1 - \omega_{\mathrm{N_2}} - \omega_{\mathrm{H_2O}}$
Boundary	**Condition**
[A]	$j_i = 0$
[B]	$j_i = 0$
[C]	$\omega_{\mathrm{H_2}} = 1 - \omega_{\mathrm{H_2O}}$
[D]	$\omega_{\mathrm{O_2}} = 1 - \omega_{\mathrm{N_2}} - \omega_{\mathrm{H_2O}}$
Source	**Term**
[3]	$\dot{m}_{\mathrm{H_2}} = \dot{m}_{\mathrm{HOR}}$
	$\dot{m}_{\mathrm{H_2O}}^{[3]} = \dot{m}_{\mathrm{PC}}^{[3]}$
[5]	$\dot{m}_{\mathrm{O_2}} = j_{\mathrm{ORR}}\left(\frac{M_{\mathrm{O_2}}}{4F}\right)$
	$\dot{m}_{\mathrm{H_2O}}^{[5]} = j_{\mathrm{ORR}}\left(\frac{M_{\mathrm{H_2O}}}{2F}\right) + \dot{m}_{\mathrm{PC}}^{[5]}$

Table 4
Parameter, boundary and initial values for EQ:10.

Domain	Important parameter
[2], [3], [5], [6]	$\sigma = \sigma_{carb}\phi_{carb}^{1.5}$
Domain	**Initial value**
[2], [3], [5], [6]	$E = 0$ V
Boundary	**Condition**
[a]	$E = 0$ V
[b]	$E = E_{Cell}$
Source	**Term**
[3]	$-j_{HOR}$
[5]	j_{ORR}

2.2.3.2. Ion flux. Ion flux is modelled similar to electron flux. Two current sources ([3] and [5]) lead to a potential field and thus a flux of ions. The potential depends on the ionic conductivity of the electrolyte. The doped PBI membrane is considered to be a porous medium filled with PAM. Conductivity is modelled as a heterogeneous mixture, which can be described by a method developed by D.A.G. Bruggeman [20]:

$$\sigma_{mix} = A\cdot\sigma_{cond.}\phi_{cond.}^{B} \tag{11}$$

where, σ_{mix} is the conductivity of the mixture. cond. refers to the conductive material and ϕ is the volume fraction of that material in the mixture. A and B are coefficients. The two cases to discuss are the conductivity within the membrane and the catalytic layers:

1. In the membrane the electrolyte is the conductive phase. Its volume fraction can be calculated from the doping level of the membrane, as seen in EQ:12. Knowing the volume fraction and the conductivity of PAM [6,8] it is possible to fit EQ:11 on literature data [21–24], obtaining the coefficients presented in EQ:13, for a doping level dependent membrane conductivity.

$$\phi_{PAM}^{[4]} = \frac{(X-1.25)\cdot V_{m,PA}}{X\cdot V_{m,PA}+V_{m,PBI}} \tag{12}$$

$$\sigma_{ionic}^{[4]} = 0.42\cdot\sigma_{PAM}(T,\omega_{PA})\cdot\phi_{PAM}^{[4]\ 2.1} \tag{13}$$

2. The volume of the catalytic layers ([3] and [5]) is shared by the solid electrode material, the electrolyte and a void fraction. In this case the ion conductivity of the electrolyte is assumed to follow the simplified Bruggeman equation, EQ:14:

Table 5
Parameter, boundary and initial values for the conservation of ionic charge.

Domain	Important parameter
[3], [4], [5]	σ_{ionic}
Domain	**Initial value**
[3], [4], [5]	$E = 0$ V
Source	**Term**
[3]	j_{HOR}
[5]	$-j_{ORR}$

Table 6
Initial conditions and parameters for EQ:16–19.

Variable	Description	Value (Ano.|Cath.)
α	Transfer coefficient	0.5|1
$x_i p$	Partial pressure reactant i	H_2|O_2
p^{ref}	Reference pressure	1 atm
γ	Pressure coefficient	0.5|1
E_A	Activation energy	(ORR: 67 kJ mol^{-1})
T^{ref}	Reference temperature	25° C
L_{cat}	Catalyst loading	0.7|1 mg cm^{-2}
d_{pt}	Diameter platinum particle	4 nm
$B_{electrode}$	Electrode thickness	50|60 nm
Θ	Platinum deactivation	0.995

$$\sigma_{ionic}^{[3]|[5]} = \sigma_{PAM}(T,\omega_{PA})\cdot\phi_{PAM}^{1.5} \tag{14}$$

2.2.4. Conservation of energy

$$\rho c_p u\nabla T = \nabla\cdot(k\nabla T)+Q \tag{15}$$

The energy balance is modelled thoroughly, including evaporation and condensation enthalpies. Due to the conditions that incoming fluxes and walls are kept at a constant temperature the maximum temperature variation experienced was below 7 K for the operating voltage of 0.35 V at 433 K. It is assumed that the effect of a non uniform temperature distribution will become more important for 3D models of the entire cell.

2.2.5. Butler–Volmer equation

The Butler–Volmer equation describes how the electric current changes with the electrode potential. Most of the source and sink terms introduced earlier depend on the current density as described by the Butler–Volmer equation:

$$j = i_0\left\{\exp\left[\frac{\alpha F\eta_{act}}{RT}\right]-\exp\left[\frac{(1-\alpha)F\eta_{act}}{RT}\right]\right\} \tag{16}$$

The modelling approach for the exchange current density, i_0, is derived from Barbir [25]. The reference exchange current density is from Weber [26] and consistent with Huang [27] and Cheddie [10], who used experimental data from Parthasarathy et al.

$$i_0 = i_0^{ref}R_{cat}\left(\frac{x_i p}{p^{ref}}\right)^{\gamma}\Theta_{active}\left[\frac{A}{m^3}\right] \tag{17}$$

$$i_0^{ref} = 5.71\times10^{-10}\exp\left[-\frac{E_A}{RT}\left(1-\frac{T}{T^{ref}}\right)\right]\left[\frac{A}{m_{pt}^2}\right] \tag{18}$$

Table 7
Parameter, boundary and initial values for EQ:20.

Domain	Important parameter
[3], [4], [5]	D_{PAM}
[3], [5]	$(A/V)_{PC}$
Domain	**Initial value**
[3], [4], [5]	$m_{PA,0}$
Source	**Term**
[3]	$\dot{m}_{PC}^{[3]}$
[5]	$\dot{m}_{PC}^{[5]}$

$$R_{cat} = \frac{6L_{cat}}{\rho_{pt} d_{pt} B_{electrode}} (1 - \Theta_{incorp}) \left[\frac{m_{pt}^2}{m_{CL}^3}\right] \quad (19)$$

R_{cat} is called electrode roughness and connects the micro geometric dimensions of the catalyst particle with the macroscopic dimensions of the catalytic layer [25,10]. The total surface area of platinum is $6L_{cat}/\rho_{pt} d_{pt} B_{electrode}$ if spherical particles of diameter d_{pt} are assumed. Its unit is area platinum per geometric volume catalytic layer. Θ_{incorp} is used to account for platinum incorporation and deactivation. Its value, being close to unity and therefore considerably reducing the active surface area, corresponds to the idea that only a small part of the catalytic layer is active [28]. The change of the electrochemical active surface area, Θ_{active}, was introduced as a relative quantity ranging from zero to unity. It modifies the exchange current density as phosphoric acid penetrates the catalytic layer. It is discussed in depth in Section 2.3.4 (Table 6).

2.3. Membrane modelling

This section describes the trans-membrane water flux in a HT-PEM FC. The resulting concentration distribution affects several sub models mentioned before. The cross over of water is described by Fick's first law, which is derived from EQ:20 for a two component system. The two mass sources represent the evaporation and condensation of water (Table 7).

$$\dot{\nabla} j_i = \left(\rho \omega_i \sum_{k=1} D_{ik} \nabla x_k\right) = R_i \quad (20)$$

2.3.1. Hertz–Knudsen equation (phase change)

It is assumed that the kinetics of a phase change can be described by the Hertz–Knudsen equation (EQ:21). The driving force is the difference in chemical potential expressed by the difference of the vapour pressure according to the liquid phase composition and the partial pressure of water in the gas phase. The 'conductivity term' the square root expression in EQ:21 is deduced from the kinetic theory of gases.

$$\dot{m}_{PC} = \left(\frac{A}{V}\right)_{PC} \left(p_{vp|PAM} - p_{H_2O}\right) \sqrt{\left(\frac{M_{H_2O}}{2\pi k_B T N_A}\right)} \quad (21)$$

The equation in its original form contains two correction factors, which in our case are simplified to unity [29]. The term $(A/V)_{PC}$ is the specific area of the vapour–liquid boundary within the geometric volume of the catalytic layer. It was estimated to be 100 [m^2/m^3] and is assumed to be constant. $p_{vp|PAM}$ is the vapour pressure of water over a PAM and depends on temperature and composition. The VLE data necessary for describing $p_{vp|PAM}$ were obtained in our laboratory and are in the process of publication. p_{H_2O} is the current partial pressure of water in the gas phase.

2.3.2. Water cross over diffusion

During FC operation water is produced at the cathode. Therefore the environment of both electrodes in terms of local humidity differ and the source terms $\dot{m}_{PC}^{[3]}$ and $\dot{m}_{PC}^{[5]}$ will cause a concentration gradient within the membrane. In order to describe this diffusive flux the diffusion coefficient of water and phosphoric acid mixtures, as seen in Fig. 4, was obtained by measurements in our laboratory and from the literature [30,31].

2.3.3. Volume fraction of a phosphoric acid mixture

The density of PAMs depends on its composition and temperature. The mass of the pure component phosphoric acid is constant, therefore a change of the density directly affects the volume (assumed negligible vapour pressure of PA up to 200 °C [16]). With increasing dilution of the solution its volume swells and thus the volume fraction of the phosphoric acid mixture within the catalytic layers changes, as described by EQ:22 and EQ:23.

$$\phi_{PAM}^{[3]} = \frac{m_{PA,0}^{[3]} + 0.5\Delta m_{PA}^{[4]}}{\rho_{PAM} \omega_{PA} V_{CL}} \quad (22)$$

$$\phi_{PAM}^{[5]} = \frac{m_{PA,0}^{[5]} + 0.5\Delta m_{PA}^{[4]}}{\rho_{PAM} \omega_{PA} V_{CL}} \quad (23)$$

$$\Delta m_{PA}^{[4]} = \Delta(\rho_{PAM} \omega_{PA}) V_4 \phi_{PAM}^{[4]} \quad (24)$$

EQ:22 shows the volume fraction of the phosphoric acid mixture in the anode. m_{PA} is the mass of pure PA, the index 0 refers to the moment of assembly. ρ_{PAM} is the density of the phosphoric acid mixture, ω_{PA} is the mass fraction of the pure component PA and V_{CL} is the volume of the catalytic layer. $\Delta m_{PA}^{[Mem]}$ is the amount of PA which gets pushed from the membrane into the electrodes due to the swelling. $\Delta(\rho_{PAM}\omega_{PA})$ describes the change of the density of PA within the membrane between operating conditions and assembly. It is assumed that the excess PA gets distributed to both electrodes equally, hence the factor 0.5 in EQ:22 and 23.

Because of the sum of all volume fractions equals unity (EQ:25), the porosity is now linked to the volume fraction of PAM as seen in EQ:27. Due to the use of the Bruggeman model the change of the porosity affects different physical properties summarized in Table 8.

$$1 = \phi_{PAM} + \phi_{solid} + \varepsilon \quad (25)$$

$$\phi_{solid} = \left(\frac{1}{\rho_{pt}} + \frac{\omega_{carb}}{\omega_{pt} \cdot \rho_{carb}}\right) \frac{m_{pt}}{V_{CL}} \approx 0.5 \quad (26)$$

$$\varepsilon(T, \omega) = 1 - \phi_{PAM}(T, \omega_{PA}) - \phi_{solid} \quad (27)$$

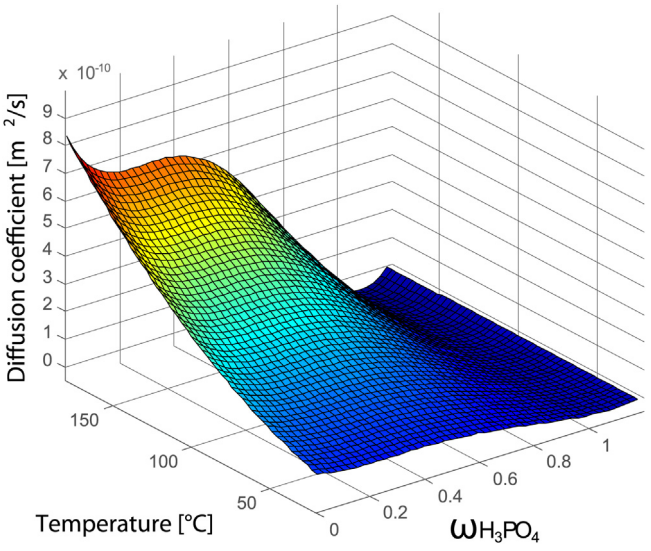

Fig. 4. Diffusion coefficient in the system water-phosphoric acid.

Table 8
Porosity effects in the CL.

Equation	Effect
Transport of mass & momentum	Porosity
Transport of species	Diffusion coefficient
Transport of ions	Conductivity
Transport of electrons	Conductivity
Transport of heat	Conductivity

An important effect of the expansion of phosphoric acid is the coverage of platinum particles in the catalytic layer and thus the reduction of ECSA, as explained in Section 2.3.4.

2.3.4. Electrochemical active surface area

In Section 2.2.5 R_{cat}, which is the total available platinum surface area per volume electrode, was deduced. However not all of that area is activated. In order to be activated the platinum particle needs to be attached to an electrically conductive surface as well as to be in contact with the ion conducting phase. As presented in Section 2.3.3 the volume fraction of the electrolyte depends on operating conditions. To account for the expansion characteristics of PAM the relative ECSA, Θ_{active}, was introduced. In Fig. 5 is shown how Θ_{active} changes as the catalytic layer gets filled with electrolyte. The catalytic area is considered to be a porous medium with two distinct pore sizes: One from the meso scale and one from the macro scale [32,33]. In addition it is assumed that PAM is wetting the electrode material. When the electrode gets loaded due to the swelling of the electrolyte the smallest capillaries get flooded first. This leads to a high penetration of the electrolyte within the CL and wetting of the surface area of the macro pores, as seen in Fig. 6. The macro pores covered with a thin film of electrolyte are considered to be activated. This condition represents maximum ECSA. With further increasing amount of PAM the activated macro pores get filled and thus inhibited and deactivated. This deactivation results from the mass transport limitation, posed by diffusion through a growing PAM layer as seen in Fig. 7. Fig. 7 is the result of Fick's first law of diffusion EQ:28 wherein J is the molar flux, δ is the diffusion length, P_i is the partial pressure, H_i the Henry coefficient of the component and $C_{0,i}$ is the concentration of the species at the catalytic surface, which is assumed to be zero.

$$J_i = -D_i \frac{1}{\delta}\left(\frac{P_i}{H_i} - C_{0,i}\right) \tag{28}$$

3. Experiment

For the validation of the numerical model polarization curves were obtained. Materials and equipment used are explained in this section whereas the results are presented in comparison to the numerical studies in Section 4.

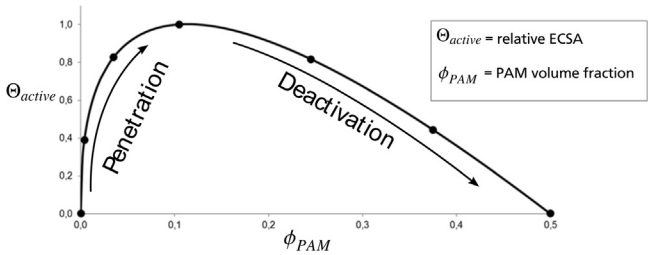

Fig. 5. Influence of the PAM expansion on the ECSA: quick penetration and activation due to loaded micro pores followed by deactivation of the macro pores.

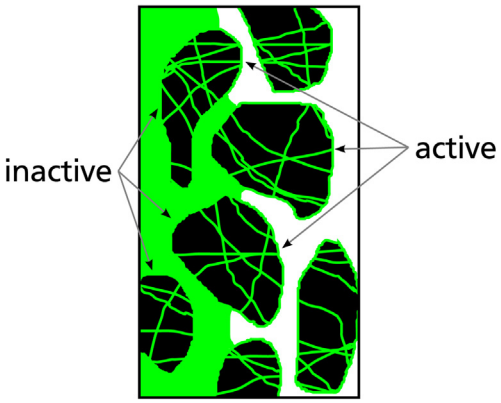

Fig. 6. Active and deactivated platinum particles.

3.1. Fuel cell test station

The fuel cell test station Evaluator C 100 by Fuel Con with the operating software FuelWork was used. The test station is capable of handling loads up to 3 kW and the heating allows operation up to 200 °C

3.2. MEA and single cell

For all experiments a BASF Celtec P 1000 MEA was used. Its properties are summarized in Table 9. The flow fields were made out of carbon with serpentine formed grooves, as seen in Fig. 1.

3.3. Procedure

After a break in, or conditioning procedure of 100 h, the polarization curves were obtained by using a voltage guided (potentiostatic) mode. Temperature and pressure sweeps were recorded. The standard operation conditions are listed in Table 10.

4. Results and discussion

4.1. Model validation

In order to validate the model a temperature and a pressure sweep was performed. The results from the simulations are shown together with corresponding experimental data in Figs. 8 and 9. For the temperature range the model predictions are in good agreement with the experiment. The pressure sweep comparison is in

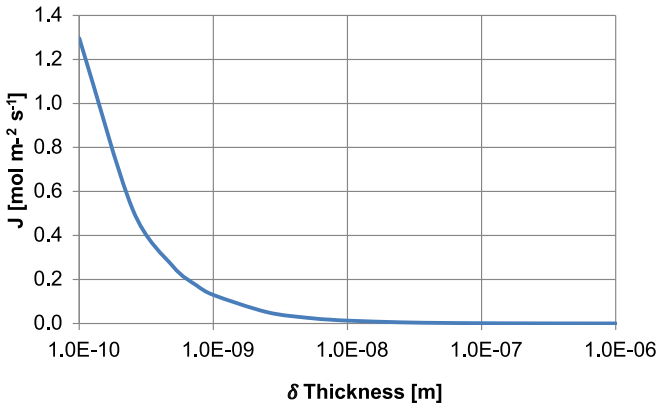

Fig. 7. Growing of the diffusion barrier with the film thickness.

Table 9
Technical specifications of the Celtec P 1000 MEA by BASF [37].

Parameter	Value
Active cell area size	45.16 cm^2
Electrode material	Woven graphite fibre
Thickness	400 μm
Cata. material	Platinum
Pt particle size	4 nm (estimated)
Cata. loading anode	0.7 mg cm^{-2}
Cata. loading cathode	1.0 mg cm^{-2}
Membrane material composition	PA doped PBI
CO tolerance	1000 ppm

Table 10
Standard operation conditions.

Parameter	Value	
	Anode	Cathode
Humidity	–	18 °C 14% r.H.
Minimum flow rate	0.025 dm^3 min^{-1}	0.3dm^3 min^{-1}
Stoichiometric factor	1.5	2.2
Temperature	160 °C	
Pressure	1 bar	

fair agreement as well, except for the overpotential region of the 3 bar polarization curve. All six *U*–*I*-curves from Figs. 8 and 9 were calculated with the same set of parameters, shown in Table 11.

4.2. Sensitivity analysis

4.2.1. Phosphoric acid content in the MEA

Fig. 10 shows the variation of the parameter PA mass in the MEA from 14.5 mg cm^{-2} to 19.8 mg cm^{-2}. Changing from 14.5 to 16.5 mg cm^{-2} yields a slight increase in performance. Any further increase of PA mass reduces the performance below the starting value and at 19.8 mg cm^{-2} the CL is flooded and the performance drops.

4.2.2. Humidity

Polarization curves with varying bubbler temperatures (cathode side) are shown in Fig. 11. With increasing humidity the performance of the fuel cell decreases. For comparison experimental data is presented as well. The experiments were carried out with a different MEA, therefore only the trends can be compared.

4.3. PA expansion

The concentration of PA depends on the temperature and on the relative humidity. Daletou [34] conducted TGAs of a doped

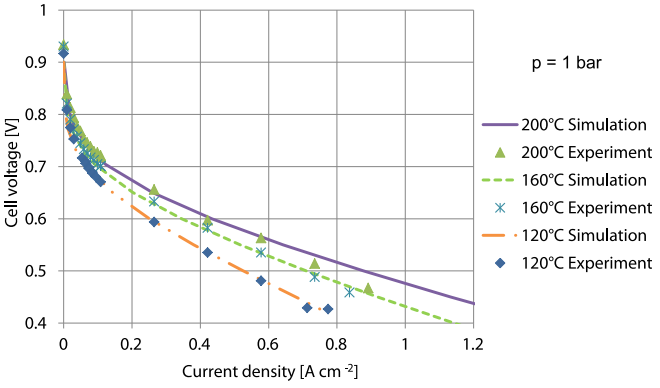

Fig. 8. Comparison: simulation and experimental data, temperature sweep.

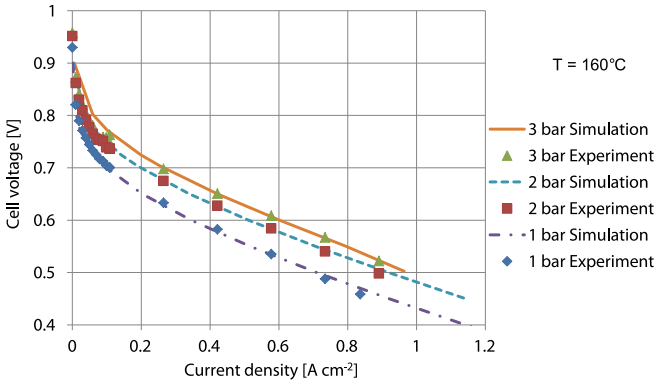

Fig. 9. Comparison: simulation and experimental data, pressure sweep.

Table 11
Simulation parameter.

Parameter	Value
Stoichiometric factor anode	1.5
Stoichiometric factor cathode	2.2
T	160 °C
P	1 bar
m_{PAM} (total)	16.5 mg cm^{-2}
m_{PAM} (in catalytic layer)	5.6 mg cm^{-2}
$\omega_{H_3PO_4}$@25 °C	0.95
Ambient humidity	14% r.H. @ 18 °C
$(A/V)_{PC}$	100 m^{-1}

PBI-membrane with varying partial pressures of water. A distinct sorption behaviour of PA was observed. At 95 °C in dry conditions the membrane has the same weight as at 160 °C with an enforced water vapour pressure of approximately 10 kPa. Under the assumption that only water evaporates during the time frame of the TGA one can conclude that PA has the same concentration at both temperatures. Furthermore neglecting the thermal expansion of liquids leads to the conclusion that the PA has the same volume as well. This important characteristic was implemented into our model as described in Section 2.3.4. During fuel cell operation the relative humidity depends on the current density ($\dot{m}_{H_2O} = j_{ORR} M_{H_2O}/(2F)$), therefore on the operating point. Fig. 12 shows the phosphoric acid redistribution during a polarization curve. Due to its expansion behaviour with increasing dilution PA moves towards the catalytic layers. As can be seen, the mass of PA in the membrane decreases and the amount in the catalytic layers increases. In sum the mass of PA does not change. In Fig. 13 the temperature dependence of the expansion behaviour is shown.

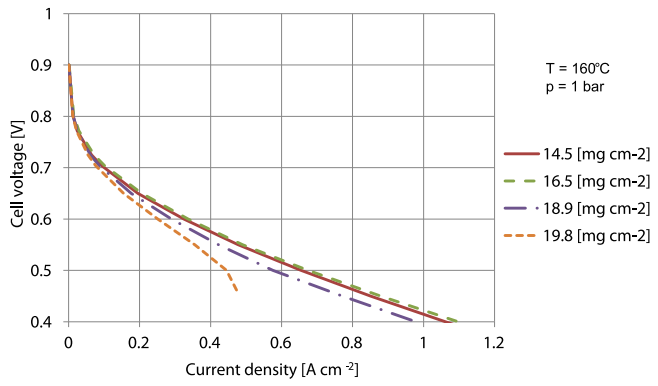

Fig. 10. Sensitivity analysis: amount of phosphoric acid in the MEA.

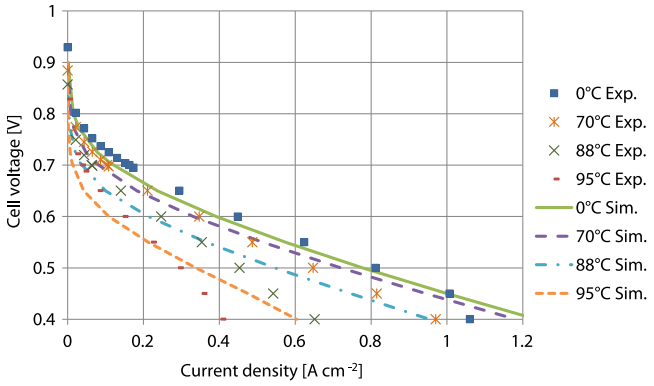

Fig. 11. Polarization curves with varying humidifier temperature (cathode).

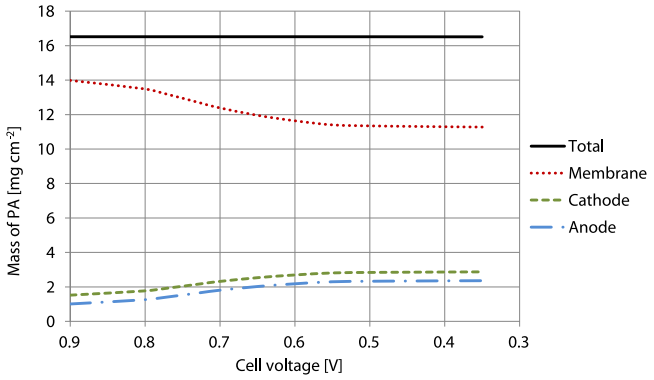

Fig. 12. Redistribution of PA within the catalytic layers during a simulation run.

The diagram is divided by vertical lines to mark a change of the inflow velocity. Due to minimum flow rates the inflow velocity for low current densities is not stoichiometric. For the anode the minimum flow rate is reached for $i = 0.105$ A cm^{-2} and at the cathode for $i = 0.53$ A cm^{-2}. As long as the current density is below these values the inflow velocities are constant (see Section 3.3). The three temperature graphs, 120 °C, 160 °C, and 200 °C, correspond to the temperature sweeps from Section 4.1. As can be seen from Fig. 13, the volume fraction of PA decreases with increasing temperature. This results from the temperature dependence of the vapour pressure of water over PAM. Combined with the actual partial pressure of water the vapour pressure is the driving force of the evaporation, hence of the volume change. Therefore the PA expansion also depends on the current density and on the flow velocity, because both affect the current humidity.

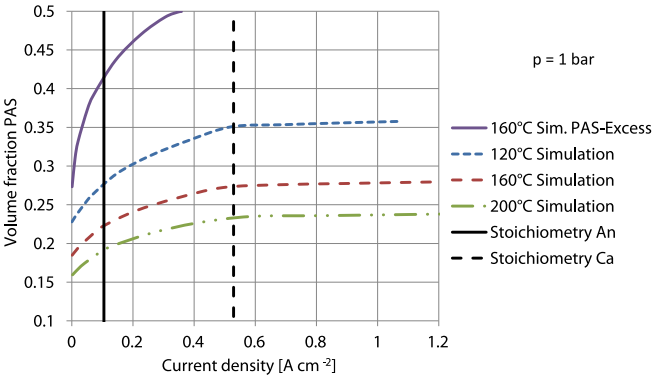

Fig. 13. Expansion of PAM in the catalytic layer at different temperatures.

4.4. Flooding

In order to analyze the behaviour of a flooded CL the mass of PAM was increased to 20 mg cm^{-2}.[3] Under operation conditions the high amount of PA leads to a water uptake, which results in a completely filled CL. The reduced performance of the FC is shown in Fig. 14 and the corresponding volume fraction in Fig. 13. Mater [35] conducted experiments with excess PAM in the MEA and found the performance to decrease with increased PAM content. By increasing the amount of PAM from 17.83 mg cm^{-2} [4] to 19.8 mg cm^{2} [4] matching results could be obtained (Fig. 15).

4.5. In-situ concentration of phosphoric acid

Highly concentrated PA under STP is hydrophilic and tends to absorb water. Because of the varying humidity within a FC, it is difficult to estimate the in-situ concentration of PAM. Our model predicts the concentrations as shown in Fig. 16. At 0.35 V cell voltage the mass fraction, ω_{PA}, ranges from 0.96 to 1.11.[4] With the following conceptual model it is possible to estimate the minimum concentration of PAM in the membrane: Consider a system containing a gas and a liquid phase as seen in Fig. 17. The liquid phase (2) is a phosphoric acid water mixture. The gas phase (1) is an inert gas with a defined water partial pressure. The pressure of the system is 1 bar and its temperature is constant at 160 °C. It is assumed that at 160 °C PA does not evaporate and that the phases are at equilibrium. Therefore the water pressure of the given PAM equals the present partial pressure of water:

$$p_{\mathrm{vp|PAM}}(T, \omega_{\mathrm{PA}}) = p_{\mathrm{H_2O}} \tag{29}$$

The water vapour pressure of the a PA-mixture with a given temperature determines the concentration of phosphoric acid.

$$\omega_{\mathrm{PA}} \sim p_{\mathrm{vp|PAM}}(T) = p_{\mathrm{H_2O}} \tag{30}$$

Assuming the gas phase consists solely of water vapour hence a partial pressure of 1 bar, the concentration can be calculated to be 86 wt%, which is the maximum dilution of phosphoric acid at 160 °C and 1 bar.

Compared to a FC operated at 1 bar and 160 °C the deduced concentration needs to be higher because the partial pressure of water is far less than the assumed 1 bar. Because a water pressure of 1 bar would mean the absence of oxygen and therefore the termination of the FC reaction. In addition, the membrane in a FC faces the moist cathode as well as the much drier anode gas. The drier condition at the anode side increases the concentration of the PAM further because of the evaporating water.

5. Assumptions revisited

5.1. Polycondensation of phosphoric acid

As explained in Section 2.1 a small and positive standard enthalpy of reaction for the first polymerization step for the temperature up to 100 °C is known. Because of the lack of further informations regarding the temperature dependence of the chemical equilibrium and the known value of $\Delta H_r^{\circ}(T < 100\,^{\circ}\mathrm{C})$ we decided to neglect the temperature influence and to use Jameson's data of the composition of PA for the discussion. It is important to revise that calculated physical properties account for the real composition due to the use of the "apparent concentration" (see Section 2.1).

[3] $\omega_{H_3PO_4} = 0.95@25\,^{\circ}\mathrm{C}$.
[4] Values higher than 1 are possible because of polycondensation.

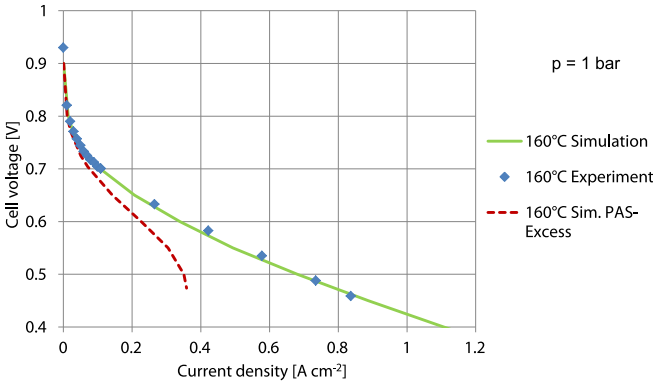

Fig. 14. Predicted performance of the flooded FC.

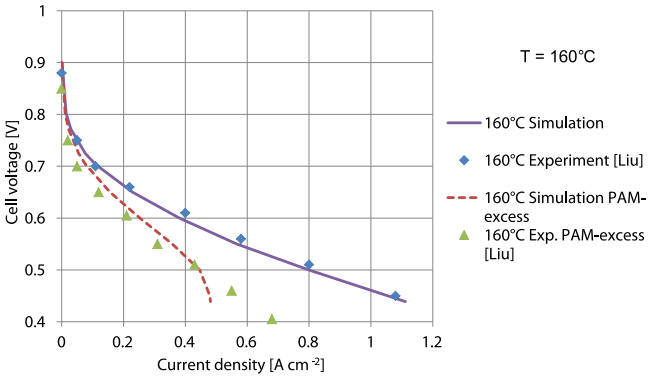

Fig. 15. Comparison: simulation and experimental data [Mater] [35].

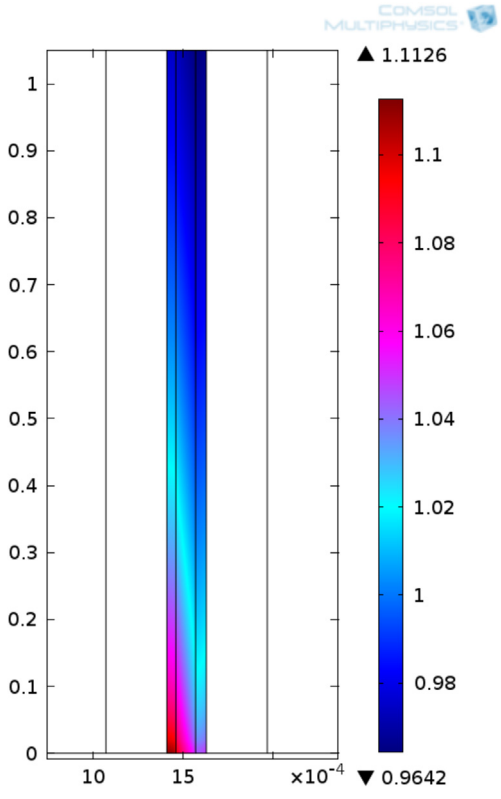

Fig. 16. In-situ concentration PAM 0.35 V.

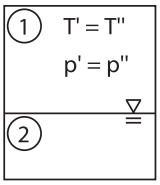

Fig. 17. Conceptual model for estimating the minimum concentration of PAM in a FC.

Table 12
Jameson: composition of the strong phosphoric acids at 15 °C [13].

H_3PO_4 [%]	P_2O_5 [%]	Ortho-	Pyro-	Tri-	Tetra or higher
≤93	67.4	100	–	–	–
102	73.9	77.1	22.1	0.79	–
113.7	82.4	7.3	23	19.3	50.4

In Fig. 16 the in-situ concentration of PAM is shown at the operating voltage of 0.35 V. The maximum concentration is located near the entrance of the dry hydrogen stream. The mean concentration calculates to 100 wt%. At this operating point the cell produces large amounts of water, which leads to a dilution of PA. Therefore in Table 13 the mean concentration of PA within the membrane for the whole polarization curve is summarized. Below 0.6 V the concentration is less than 102 wt% PA. Following Jameson, phosphoric acid with this concentration still consists of 77.1 wt% ortho-PA (Table 12). Especially at lower operating voltages and higher temperatures polymerization might occur. It seems necessary to further investigate the effects of polycondensation regarding the physical properties of highly concentrated phosphoric acid containing poly-phosphoric acids.

5.2. Volume swelling of the PBI-membrane

The thickness of the membrane depends on the acid content [17]. Fig. 13 shows the amount of phosphoric acid in the membrane during a polarization curve. As described in Table 13, 20% of the mass of phosphoric acid leave the membrane towards the CL. It is to be expected that this amount will change the thickness of the membrane, which until now is not accounted for.

6. Conclusion

A 2D FEM model of a HT-PEM fuel cell was built and enhanced by adding the vapour liquid equilibrium and evaporation kinetics into the coupled system. Thereby the substance distribution of water respectively phosphoric acid was computed and used for

Table 13
Cell voltage, current density, mass density of PA in the membrane and its mean concentration during a polarization curve simulation.

U_{Cell} [V]	i [A cm^{-2}]	$m_{PA,Mem}$ [mg cm^{-2}]	Ø ω_{PA} [wt%]
0.9	0.00	13.98	114
0.80	0.01	13.50	111
0.77	0.03	13.20	110
0.72	0.07	12.66	107
0.70	0.10	12.43	106
0.65	0.21	11.96	104
0.6	0.34	11.65	102
0.55	0.49	11.41	101
0.5	0.67	11.35	101
0.45	0.88	11.32	101
0.4	1.10	11.30	100
0.35	1.33	11.28	100

determination of physical properties while solving the model. The in situ concentration of phosphoric acid was found to be in the range of 96 to 111 wt%.

Polarization curves for different temperature and pressure sweeps was simulated and compared to the experimental data. The model showed consistency and was used to investigate the sorption behaviour further. The simulation is able to predict the effects of excess acid as investigated by Liu [35]. The following conclusion can be drawn:

Humidity strongly affects the performance of high temperature fuel cells. The growing of the acid film layer due to sorption can cause severe mass transport limitations. This effect can be reduced by increasing the temperature, which leads to an increased vapour pressure of water and a higher concentration. Reducing the partial pressure of water in the gas phase by lowering the current density resp. the water production has the same effect. As the intended application for high temperature fuel cells is the operation with an upstream steam reformer and therefore high humidity conditions, the investigation of the water balance is of great importance.

Regarding the effects of humidification and flooding it is important to point out that the condition of the MEA is crucial for the result. Obviously when diluted the ionic conductivity of PA increases.[5] Many publications observed the effects of humidification with differing system responses [34–36]. The discrepancy whether increasing the humidity of a HT fuel cell increases the performance or not depends on the content of PA in the catalytic layer. An increase in performance as observed by Daletou [34] might, in addition to the increased ionic conductivity, be the effect of a lack of PA within the CL. With increasing expansion of PA due to sorption of water more catalytic particle are connected to the electrolyte phase and the ECSA grows.

The opposite effect as described by Liu [35] and Lobato [36] and also observed by our bachelor student M. Bahr (Fig. 11) might be caused by a higher amount of PA in the CL which leads to decent performance under unhumidified conditions. But the expanded PA during humidified operation will pose a deactivation of ECSA and hence a decrease in performance.

This work is intended to be the basis for future publications regarding degradation due to water stress and 3D simulations for determining the water discharge rate at the anode. Furthermore we are preparing the publication of our VLE measurements regarding the vapour pressure of phosphoric acid and the vapour pressure of water in the presence of phosphoric acid.

References

[1] Bundesumweltministerium (BMU), Energiekonzept: für eine umweltschonende, zuverlässige und bezahlbare Energieversorgung, 2010.
[2] S. Malhotra, J. Electrochem. Soc. 144 (2) (1997) L23, http://dx.doi.org/10.1149/1.1837420.
[3] Q. Li, J.O. Jensen, R.F. Savinell, N.J. Bjerrum, Prog. Polym. Sci. 34 (5) (2009) 449–477, http://dx.doi.org/10.1016/j.progpolymsci.2008.12.003.
[4] J.A. Asensio, E.M. Sánchez, P. Gómez-Romero, Chem. Soc. Rev. 39 (8) (2010) 3210, http://dx.doi.org/10.1039/b922650h.
[5] J. Zhang, Z. Xie, J. Zhang, Y. Tang, C. Song, T. Navessin, Z. Shi, D. Song, H. Wang, D.P. Wilkinson, Z.-S. Liu, S. Holdcroft, J. Power Sources 160 (2) (2006) 872–891, http://dx.doi.org/10.1016/j.jpowsour.2006.05.034.
[6] D.-T. Chin, H.H. Chang, J. Appl. Electrochem. 19 (1989) 95–99.
[7] E.L. Holt, P.A. Lyons, J. Phys. Chem. 69 (7) (1965) 2341–2344, http://dx.doi.org/10.1021/j100891a037.
[8] D.I. MacDonald, J.R. Boyack, J. Chem. Eng. Data 14 (3) (1969) 380–384.
[9] T. Sousa, M. Mamlouk, K. Scott, Chem. Eng. Sci. 65 (8) (2010) 2513–2530, http://dx.doi.org/10.1016/j.ces.2009.12.038.
[10] D. Cheddie, N. Munroe, Int. J. Hydrogen Energy 32 (7) (2007) 832–841, http://dx.doi.org/10.1016/j.ijhydene.2006.10.061.
[11] C. Siegel, Energy 33 (9) (2008) 1331–1352, http://dx.doi.org/10.1016/j.energy.2008.04.015.
[12] D. Cheddie, N. Munroe, J. Power Sources 147 (1–2) (2005) 72–84, http://dx.doi.org/10.1016/j.jpowsour.2005.01.003.
[13] R.F. Jameson, J. Chem. Soc. (Resumed) (1959) 752, http://dx.doi.org/10.1039/JR9590000752.
[14] R.A. Munson, J. Phys. Chem. 69 (5) (1965) 1761–1762, http://dx.doi.org/10.1021/j100889a514.
[15] R.A. Munson, J. Phys. Chem. 68 (11) (1964) 3374–3377, http://dx.doi.org/10.1021/j100793a045.
[16] E.H. Brown, C.D. Whitt, J. Ind. Eng. Chem. 44(3) (1952) 615–618.
[17] R. He, Q. Li, A. Bach, J. Jensen, N. Bjerrum, J. Membr. Sci. 277 (1–2) (2006) 38–45, http://dx.doi.org/10.1016/j.memsci.2005.10.005.
[18] B.E. Poling, J.M. Prausnitz, J.P. O'Connell, The Properties of Gases and Liquids, fifth ed., McGraw-Hill, New York, 2001.
[19] R.B. Bird, W.E. Stewart, E.N. Lightfoot, Transport Phenomena, second ed., J. Wiley, New York, 2002.
[20] D.A.G. Bruggeman, Ann. Phys. 416 (7) (1935), 636–664, http://dx.doi.org/10.1002/andp.19354160705
[21] M.-Q. Li, Z.-G. Shao, K. Scott, J. Power Sources 183 (1) (2008) 69–75, http://dx.doi.org/10.1016/j.jpowsour.2008.04.093.
[22] Y.-L. Ma, J.S. Wainright, M.H. Litt, R.F. Savinell, J. Electrochem. Soc. 151 (1) (2004) A8, http://dx.doi.org/10.1149/1.1630037.
[23] V. Kurdakova, E. Quartarone, P. Mustarelli, A. Magistris, E. Caponetti, M. Saladino, J. Power Sources 195 (23) (2010) 7765–7769, http://dx.doi.org/10.1016/j.jpowsour.2009.09.064.
[24] T.-H. Kim, T.-W. Lim, J.-C. Lee, J. Power Sources 172 (1) (2007) 172–179, http://dx.doi.org/10.1016/j.jpowsour.2007.07.040.
[25] F. Barbir, PEM Fuel Cells: Theory and Practice, Elsevier Academic, Amsterdam and London, 2005.
[26] A.Z. Weber, J. Newman, SIAM J. Appl. Math. 70 (2) (2009) 488–509, http://dx.doi.org/10.1137/08071973X.
[27] J.C. Huang, R.K. Sen, E. Yeager, J. Electrochem. Soc. 126 (5) (1979) 786, http://dx.doi.org/10.1149/1.2129139.
[28] J. Zhang, PEM Fuel Cell Electrocatalysts and Catalyst Layers, 2008, Springer London, London.
[29] R. Marek, J. Straub, Int. J. Heat Mass Transf. 44 (2001) 39–53.
[30] O.W. Edwards, E.O. Huffman, J. Phys. Chem. 63 (11) (1959) 1830–1833, http://dx.doi.org/10.1021/j150581a011.
[31] D.G. Leaist, P.A. Lyons, J. Sol. Chem. 13 (2) (1984) 77–85, http://dx.doi.org/10.1007/BF00646041.
[32] J. Lobato, M. Rodrigo, J. Linares, K. Scott, J. Power Sources 157 (1) (2006) 284–292, http://dx.doi.org/10.1016/j.jpowsour.2005.07.040.
[33] J.-H. Kim, H.-J. Kim, T.-H. Lim, H.-I. Lee, J. Power Sources 170 (2) (2007) 275–280, http://dx.doi.org/10.1016/j.jpowsour.2007.03.082.
[34] M.K. Daletou, J.K. Kallitsis, G. Voyiatzis, S.G. Neophytides, J. Membr. Sci. 326 (1) (2009) 76–83, http://dx.doi.org/10.1016/j.memsci.2008.09.040.
[35] S. Matar, A. Higier, H. Liu, J. Power Sources 195 (1) (2010) 181–184, http://dx.doi.org/10.1016/j.jpowsour.2009.06.084.
[36] J. Lobato, P. Cañizares, M.A. Rodrigo, J.J. Linares, D. Úbeda, F.J. Pinar, Fuel Cells 10 (2) (2010) 312–319, http://dx.doi.org/10.1002/fuce.200900088.
[37] T.J. Schmidt, J. Baurmeister, J. Power Sources 176 (2) (2008) 428–434, http://dx.doi.org/10.1016/j.jpowsour.2007.08.055.

[5] For $\omega_{PA} > 0.5$.